Building and Environment 46 (2011) 2060–2068

Contents lists available at ScienceDirect

Building and Environment

journal homepage: www.elsevier.com/locate/buildenv

Combining hygrothermal and corrosion models to predict corrosion of metal fasteners embedded in wood

Samuel L. Zelinka [a,*], Dominique Derome [b], Samuel V. Glass [c]

[a] USDA Forest Products Laboratory, One Gifford Pinchot Drive, Madison, WI 53726, USA
[b] Empa-Swiss Federal Laboratory for Materials Science and Technology, 8600 Dübendorf, Switzerland
[c] USDA Forest Products Laboratory, One Gifford Pinchot Drive, Madison, WI 53726, USA

ARTICLE INFO

Article history:
Received 6 January 2011
Received in revised form
11 April 2011
Accepted 11 April 2011

Keywords:
Corrosion
Hygrothermal modeling
Decks
Wood preservatives

ABSTRACT

A combined heat, moisture, and corrosion model is presented and used to simulate the corrosion of metal fasteners embedded in solid wood exposed to the exterior environment. First, the moisture content and temperature at the wood/fastener interface is determined at each time step. Then, the amount of corrosion is determined spatially using an empirical corrosion rate model and the inputs of the first step. The result is a corrosion profile along the length of the fastener generated by summing the corrosion depths determined at each time step. We apply the combined model to predict the annual corrosion depth along a metal fastener in wood decks situated in nine different US cities. Corrosion profiles are found to exhibit the same general shape independently of climatic load, with the largest amount of corrosion occurring at 1–5 mm from the wood surface with corrosion depths ranging from 5 μm in Phoenix, Arizona to 45 μm in Hilo, Hawaii. Corrosion is confined to the first 7–20 mm of the fastener below the wood surface. By varying the climatic loads, we find that although there is a definite relation between total annual rain and total annual corrosion, under the same rain loads corrosion is higher for a climate with more evenly distributed rain events. The proposed combined model is able to capture corrosion behavior under varying loading. A sensitivity analysis gives guidelines for future corrosion modeling work for fasteners in wood.

Published by Elsevier Ltd.

1. Introduction

Wood structures that are exposed to the exterior environment, like terrace decks, balconies, playground equipment, etc., are susceptible to moisture damage such as wood rot and metal corrosion. Frequently, softwoods (pine, spruce) are treated with wood preservatives to be durable and suitable for these exterior applications. The durability of treated wood depends not only on protecting the wood from biological attack but also on minimizing the corrosion of embedded fasteners. The corrosion rate of embedded fasteners depends on the moisture and temperature conditions at the metallic surface, which fluctuate considerably in outdoor wood constructions considered here. In this paper, we present a modeling approach that combines heat and mass transport in the wood exposed to environmental loading with corrosion of the metallic fasteners in contact with the wood.

The specific context of this paper stems from a wood preservation regulation change that occurred in the United States in January 2004. Alkaline copper quaternary (ACQ) and copper azole (CuAz) replaced chromated copper arsenate (CCA) in residential applications [1]. These alternative wood preservatives were suspected to be more corrosive to embedded metal fasteners than CCA [2,3]. Since the regulation change, the corrosiveness of CuAz and ACQ has been evaluated in several laboratory tests. Most of this work used the American Wood Protection Association AWPA E-12 standard, which places metal coupons between blocks of wood at 49 °C and 90% relative humidity (RH) for at least 240 h [4,5]. Other procedures using more realistic temperatures were developed. Kear et al. [5] exposed fasteners embedded in treated wood at 21 °C to 3 different relative humidities ranging from 75% to 98% RH for 1 year. Zelinka and Rammer [6] embedded fasteners in blocks of treated wood exposing them to 27 °C and 100% RH for one year. Furthermore, electrochemical tests in a water-extract of treated wood were found to have the same corrosion rates as those measured at the 27 °C 100% RH conditions [7]. These tests all show that ACQ and CuAz are more corrosive than CCA. However, due mainly to the variations of testing conditions, the measured corrosion rates from these tests have a wide range of values, for example, from 2 to113 μm yr^{-1} for hot-dip galvanized steel in ACQ-treated wood (1–26 μm yr^{-1} for CCA). As the corrosion rate of

* Corresponding author. Tel.: +1 608 231 9277; fax: +1 608 231 9592.
E-mail address: szelinka@fs.fed.us (S.L. Zelinka).

0360-1323/$ – see front matter Published by Elsevier Ltd.
doi:10.1016/j.buildenv.2011.04.017

metals in contact with wood is known to depend on the moisture content and temperature conditions at the interface, in-service conditions along the interface are needed for durability prediction. In-service moisture content (MC, the ratio of the mass of water to the mass of oven dry wood) of wood decks experience large fluctuations (from 8% to 80% MC) and non uniform distribution depending on the environmental conditions [8,9]. Therefore a steady-state approximation of the MC conditions or of the corrosion rate would not be able to capture these changes and could not lead to prediction of corrosion lifetime.

For predicting the corrosion lifetime of fasteners in treated wood, we propose to predict the corrosion rate using the conditions at the wood/fastener interface determined under environmental conditions by combining a heat and moisture transport model with a corrosion model. An existing, validated heat and moisture transport model [10] is used to calculate the conditions at the wood–fastener interface with a complete set of climatic data applied as boundary conditions including air temperature and relative humidity, rain precipitation, and wind conditions[1]. The corrosion of the embedded fastener is computed from the calculated temperature and moisture content at the wood–fastener interface at each time step. In the next section, we describe this modeling approach, including the geometry of the application problem and the determination of the required material properties. In Section 3, we use this modeling approach in comparing the corrosion depth profiles of fasteners for constructions under 9 different climatic conditions and present the results of this study. In Section 4, we discuss two key aspects of this study: the selection of the appropriate year of climatic data and sensitivity of the results to variations of the three parameters of the corrosion model.

2. Combined heat, moisture, and corrosion model

2.1. Geometry of the physical problem

Similarly to most of the previous work on corrosion in treated wood, which has focused on residential decks, we simulate the corrosion of the fastener that connects the decking to the joists (i.e. a deck screw). The American Forest and Paper Association recently published a Prescriptive Residential Wood Deck Construction Guide based on the 2009 International Residential Code (IRC) which gives the minimum construction requirements for single level residential wood decks. The guide specifies an “8d” nail (64 mm long, ~3 mm in diameter), 38 mm thick deck boards spaced 3.2 mm apart, and 38 mm thick joists.

In this work, two simplifications are made to the configuration. The geometry and meshing of the calculation domain are shown in Fig. 1. The first simplification is that the fastener is modeled within a single wood member, which can be thought of as a joist with the deck board removed. The second simplification is that the problem can be treated two-dimensionally, which is equivalent to assuming that the fastener is in the middle of an infinitely long joist. Symmetry considerations are used so that only half of the width needs to be modeled. The two dimensional mesh is 20 by 90 mm and consists of 1965 wood elements, of exponentially decreasing size going toward the exterior boundaries and nail interface, 336 steel elements and 2400 nodes. Heat transport was simulated in the nail to account for possible thermal bridging effects; however, the nail was assumed to be impermeable to moisture and had no moisture capacity.

[1] The model is also able to account for solar radiation, although in this paper, its effect was not considered. A further explanation is given in Section 3.1.

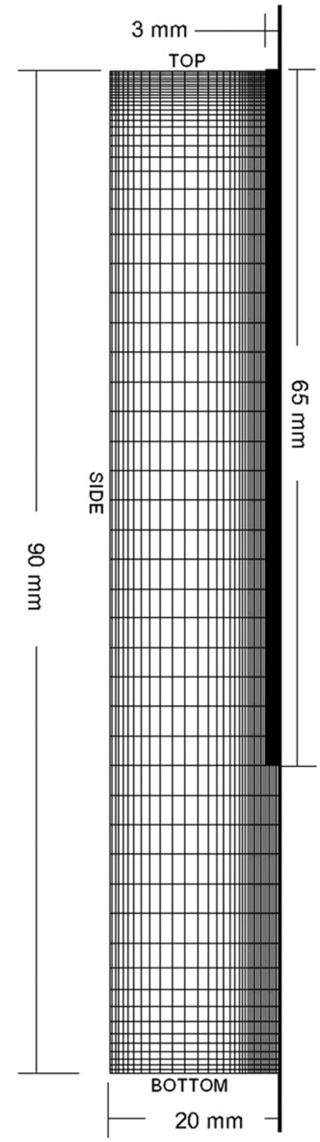

Fig. 1. Calculation mesh (domain) used in the simulations with physical dimensions. The elements with steel material properties are black to clearly identify the nail. Top, side and bottom refer to the boundary conditions, e.g. exposed to environmental conditions. The heavy line represents the symmetry plane.

2.2. Corrosion model

It is believed that the corrosion mechanism for metals embedded in wood is aqueous [11–14] and many researchers have observed a threshold moisture content (between 15 and 20%) below which corrosion in wood does not occur [11,12]. This parallels the mechanism in atmospheric corrosion, where a liquid film is required for corrosion. The simplest such model for calculating the risk of atmospheric corrosion is found in the ISO 9223 standard and assumes that a liquid film capable of causing corrosion forms when the relative humidity is greater than 80% and the temperature is greater than the freezing temperature of water (0 °C) [15]. Our empirical corrosion model maintains this temperature threshold for corrosion, but includes the dependence of the corrosion rate on moisture content above the corrosion temperature threshold.

Short and Dennis used electrochemical techniques to measure the corrosion rate of zinc as a function of moisture content [12]. They placed a small strip of CCA treated wood between a stainless steel counter electrode and a zinc working electrode. Two more pieces of wood were placed on the outside of the working and counter electrodes to create a “sandwich”. The wood moisture content was adjusted by placing the assembly in various conditioning chambers and the corrosion rate was measured at 11 different moisture contents using polarization resistance. The relationship between polarization and the corrosion rate was explored first by Mansfeld [16] and this relationship has been recently exploited to study a diverse range of phenomena such as the corrosion of rebar in concrete [17–19]. The polarization resistance data indicated a sigmoidal dependence of the corrosion rate on moisture content between 15 and 27% MC. In addition, below 15% MC, there was no corrosion and above 27% MC, the corrosion rate was constant at its maximum value. We have fit their experimental corrosion rate data (R, μm yr^{-1}) as a function of moisture content, M (kg kg^{-1} expressed as a percentage), with:

$$R = \frac{A}{1+e^{B(C-M)}} \quad (1)$$

where A represents the maximum corrosion rate (μm yr^{-1}), B represents the steepness of the transition from 0 to A, and C represents the moisture content at which $R = A/2$, i.e. a metric of the moisture content threshold of corrosion. The parameters B (0.83) and C (24) are taken from our fit of the published data of Short and Dennis [12]. The parameter A, which is physically the asymptotic corrosion limit, is taken as 52.3 μm yr^{-1} from recent electrochemical measurements of hot-dip galvanized steel in an extract of ACQ-treated southern pine [7]. A graph of the corrosion rate as a function of moisture content is shown in Fig. 2, with the data of Short and Dennis overlaid [12] (scaled to the maximum corrosion found by Zelinka et al. [7]).

There are no data on the temperature dependence of corrosion in treated wood. However, since the corrosion mechanism in wood is believed to be aqueous, it is unlikely that corrosion occurs below freezing. Therefore our model enforces a “no-corrosion” condition when the wood near the metal surface is less than 0 °C, similar to the ISO 9223 model [15].

2.3. Heat and moisture transport model

The coupled heat and moisture transport is calculated using an existing, validated heat and moisture transport model implemented with a finite element code [10,20,21] which uses capillary pressure, p_c, as the driving potential for moisture transport. The governing equations are:

$$\frac{\partial w}{\partial p_c}\frac{\partial p_c}{\partial t} = -\nabla^{\mathrm{T}}\left(\mathbf{g}_{m,l}+\mathbf{g}_{m,v}\right) \quad (2)$$

$$(c_o\rho_o + c_l w)\frac{\partial T}{\partial t} + \left(c_l T\frac{\partial w}{\partial p_c}\right)\frac{\partial p_c}{\partial t} = -\nabla^{\mathrm{T}}\left(\mathbf{g}_{h,c}+\mathbf{g}_{h,a}\right) \quad (3)$$

$$\mathbf{g}_{m,l} = -\mathrm{K}_l\nabla p_c \quad (4)$$

$$\mathbf{g}_{m,v} = -\frac{\delta_v p_v}{\rho_l R_v T}\nabla p_c - \frac{\delta_v p_v}{\rho_l R_v T^2}\left(\rho_l L_v + p_c\left(T^\gamma - 1\right)\right)\nabla T \quad (5)$$

$$\mathbf{g}_{h,c} = -\lambda\nabla T \quad (6)$$

$$\mathbf{g}_{h,a} = (c_l T)\mathbf{g}_{m,l} + (c_v T + L_v)\mathbf{g}_{m,v} \quad (7)$$

where

w is volumetric moisture content [kg m^{-3}]
t is time [s]
T indicates the transpose
$\mathbf{g}_{\mathrm{m}}$ is moisture flux [kg m^{-2} s^{-1}], and the subscripts l and v stand for liquid and vapor, respectively
c is specific heat [J kg^{-1} K^{-1}], and the subscript 0 stands for dry solid
ρ is density [kg m^{-3}]
T is absolute temperature [K]
$\mathbf{g}_{\mathrm{h}}$ is heat flux [W m^{-2}], and the subscripts c and a stand for conductive and advective, respectively
K_l is liquid water permeability [s]
δ_v is vapor permeability [s]
p_v is vapor pressure [Pa]
R_v is the specific gas constant for water vapor [J kg^{-1} K^{-1}]
L_v is heat of vaporization [J kg^{-1}]
γ is the derivative with respect to temperature of the surface tension normalized to the surface temperature at a reference temperature [K^{-1}]
λ is thermal conductivity [W m^{-1} K^{-1}]

The model can handle the full range of moisture content of wood from dry to capillary saturation as it includes liquid transport. The non-linearity as well as the temperature and moisture content dependence of the material properties are implemented. Time stepping is adaptive while the temperature and moisture content of the wood at each node are written to an output file at 1 h intervals.

2.3.1. Boundary conditions

To simulate the moisture conditions of a deck, atmospheric boundary conditions including air temperature and relative humidity, precipitation, and wind dependent convective heat and mass transfer coefficients are applied on the top surface. Precipitation is applied as an hourly average liquid thickness of rain, snow is treated as its liquid water equivalent. On the “side” and “bottom” surfaces (Fig. 1), only the air temperature and relative humidity are taken from the climatic data while the convective heat and mass transfer coefficients are taken as constant (20 W m^{-2} K^{-1}and 2.4 × 10^{-8} s m^{-1}, respectively).

2.3.2. Material properties

The accuracy to which the hygrothermal model can predict the wood moisture content, and thus the corrosion rate, is dependent on appropriately determined material properties, namely: full

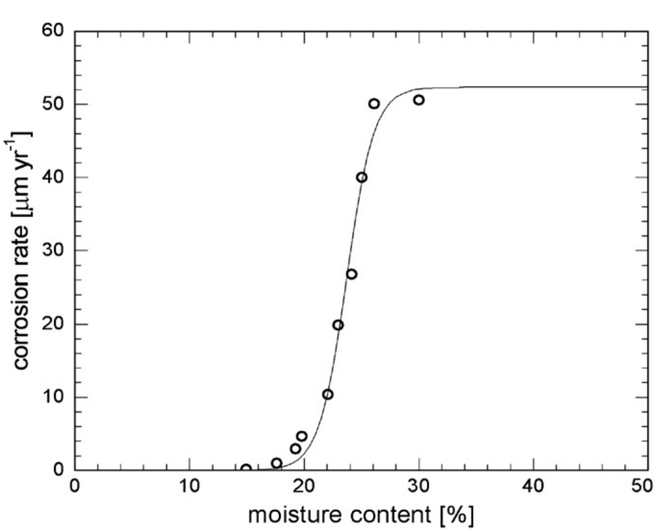

Fig. 2. Corrosion model used in this study derived from Refs. [7] and [12].

moisture retention curve over both the hygroscopic (sorption isotherm) and overhygroscopic regimes, moisture diffusivity (from vapor permeability and liquid water conductivity), thermal conductivity, and heat capacity. In this work, the moisture retention curve and diffusivity are functions of capillary pressure, the thermal conductivity is a function of moisture content, and the heat capacity is a constant. No temperature dependency is included at this stage of the work.

There are few published measurements on the hygrothermal properties of treated southern pine. Sorption isotherms of preservative-treated and untreated southern pine have recently been published [22] and there were only small differences between the isotherms of ACQ, CCA, and untreated southern pine. However, the vapor permeability of treated wood, its liquid water conductivity, and its moisture retention curve in the overhygroscopic regime have not been characterized.

In the present work, the material properties are taken from work on untreated Scots pine (*Pinus sylvestris*) [23]. While it is likely that there are differences in the hygrothermal properties of Scots pine and southern pine, the data were chosen because of the quality and completeness of the data and because the data are from the same genus. The liquid, vapor, and total permeabilities were taken from measurements in the tangential direction, and utilized the diffusivity approach presented by Carmeliet et al. [24]. Heat capacities and thermal conductivity values for loblolly pine (*Pinus taeda*) were taken from the *Wood Handbook* [25]. The sensitivity of the model to these properties has been examined previously [26].

2.4. Combining models

Modeling the corrosion of fasteners in treated wood involves two steps: first, calculating the wood moisture content and temperature at the wood–metal interface; and second, calculating the metal corrosion rate, which is dependent on this moisture content. We calculate the corrosion rate at each output time step (every hour) at each node along the wood–metal interface from Eq. (1) and the wood moisture content. We assume the corrosion rate to be constant over the entire following hour. If the temperature of the wood at the interface is less than zero for a given hour, the corrosion rate at that node is set to zero. The total amount of corrosion during the simulation is found by summing the amounts determined hourly.

Since combining the models does not introduce additional physical models, validation of the combined model reduces to a validation of the hygrothermal model and the corrosion model separately. The hygrothermal model has been validated previously [10] and the corrosion model is empirical.

In the next section we apply the combined models approach for a parametric study.

3. Examination of the corrosion potential in different US climates

Corrosion in outdoor structures is expected to depend upon climate. Intuitively, it should depend upon the amount of precipitation, the way in which precipitation is distributed over time, drying potential, temperature, and possibly other climatic variables. Drying potential likely depends on temperature, humidity, solar radiation, and wind speed.

To examine the possibility for corrosion in different climates, we apply the combined models approach to 9 cities in the USA. The cities are chosen based on the climate zones proposed by Briggs et al. [27] which have been adopted by the American Society of Heating, Refrigerating and Air-Conditioning Engineers (ASHRAE) and the International Energy Conservation Code (IECC). The methodology splits the continental United States into seven zones (1–7) based upon temperature; each of these temperature zones is then assigned a moisture classification, “a” for humid, “b” for dry, or “c” for coastal. Eight cities from the continental United States are examined, from six of the seven climate zones, including all moisture subclassifications (Table 1 and Fig. 3). Additionally, Hilo, HI is chosen to simulate corrosion in what was expected to be an extreme environment (more than 5 m of annual rainfall).

3.1. Climatic data

The climatic data for the simulations are obtained from the Solar and Meteorological Surface Observation Network (SAMSON) dataset which includes hourly weather observations for 237 weather stations throughout the US during the period 1961–1990 [28], including the nine locations selected above. It would have been possible to use the whole set of 30 years to perform the simulations. A more common approach is the selection of the dataset of a specific year, based on one or several criteria of particular relevance for the problem studies. Examples of such selection in building physics deal mainly with the hygrothermal behavior of wall assemblies. For example, ASHRAE 160 recommends 10th percentile hottest and coldest years as moisture design reference years [29]. We ran the combined hygrothermal/corrosion model in preliminary simulations with several reference years proposed for wall assemblies [29,30]. We found that these reference years do not result in large amounts of corrosion compared to other years. This may be expected as wall assemblies and terrace decks experience very different boundary conditions and hygrothermal gradients.

During preliminary simulations, we observed that the climatic parameter that has the most impact on the total corrosion depth is rain. Thus, the reference years are selected based upon precipitation, using two rain parameters as simplified simulations [26] show that the amount of corrosion is sensitive to both the total amount of

Table 1
Cities chosen and summary of the climatic data used in the simulations.

Zone	City	State	Year	Maximum predicted corrosion depth (μm)	Yearly		Total number of hours with	
					Mean temp. (°C)	Total rainfall (m)	$T > 0$ °C	Rain
1	Hilo	HI	1990	45	23.0	5.36	8760	2213
1	Miami	FL	1968	12	23.4	2.12	8760	588
2a	New Orleans	LA	1961	20	19.6	2.12	8715	593
2b	Phoenix	AZ	1978	05	23.3	0.39	8734	284
3a	Atlanta	GA	1975	17	15.9	1.68	8440	699
4a	Baltimore	MD	1989	16	12.6	1.32	8127	794
4c	Seattle	WA	1971	26	10.1	1.10	8422	1205
5a	Chicago	IL	1983	11	9.7	1.25	6691	739
6a	Minneapolis	MN	1983	12	7.8	0.99	6217	731

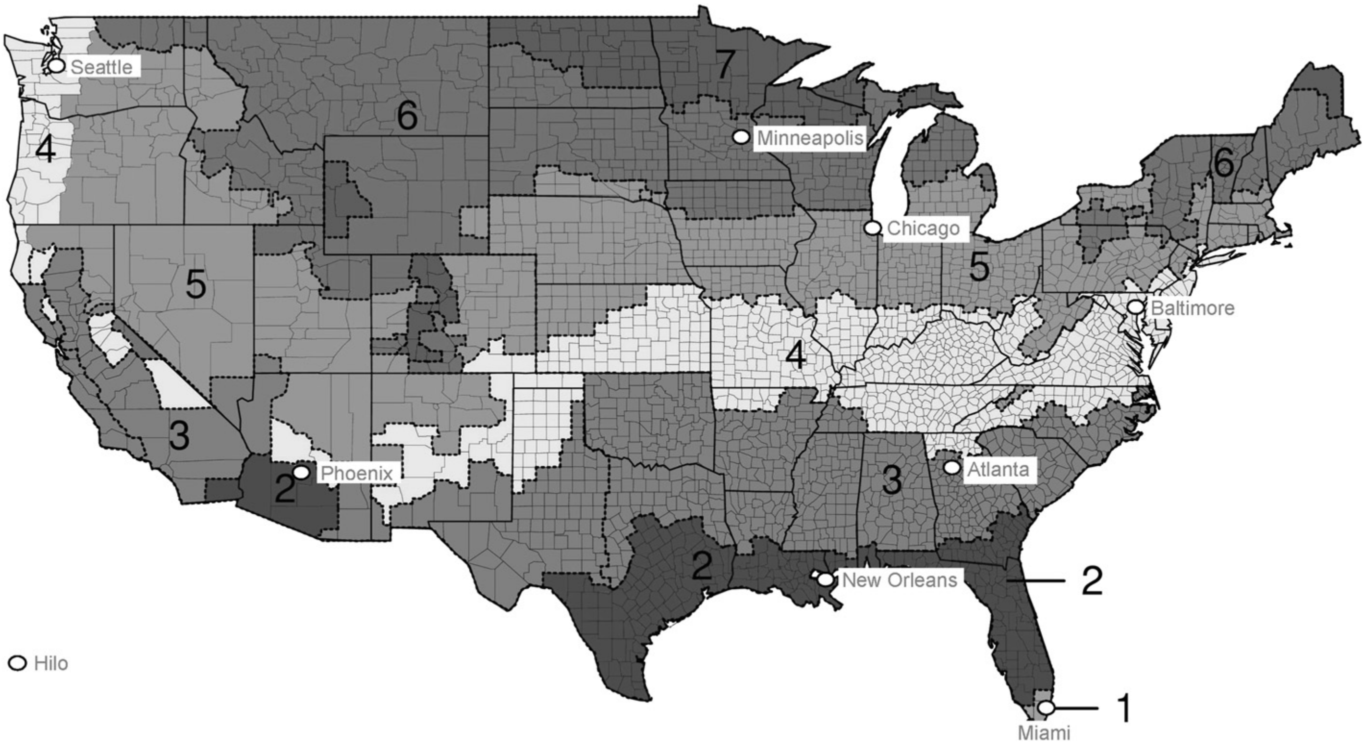

Fig. 3. Map of climate zones proposed by ASHRAE and IECC (reprinted with permission from the Building Energy Codes Resource Center).

annual rainfall as well as the number of hours with a rain event. For each city, the years 1961–1990 are ranked based upon the total amount of annual precipitation. From this list, the top five years are selected and the hourly data are analyzed for the number of hours with non-zero precipitation. From the five analyzed years, the year with the most hours of rain is selected as the reference year. The reference years selected by this method from the SAMSON dataset are given in Table 1. To simulate a worst case scenario for corrosion, e.g. a deck that is constantly in the shade, solar radiation is excluded from the climatic data. The years selected, along with some rainfall and temperature mean or total values, are included in Table 1.

3.2. Results of the simulations

Simulations are run for one calendar year for each city, starting in January. The starting temperature of the wood and metal is set to be equal to the air temperature at the first time step and the starting moisture content is 13%. The results of the one year simulation for each city are shown in Fig. 4, where the amount of corrosion is given as a function of the depth below the wood surface.

The curves in Fig. 4 have several features in common: the total corrosion penetration increases with depth for the first few millimeters, reaches a maximum, and then decreases with depth until it reaches zero. The similarities between these curves can be explained by the physics of the phenomenon. During a rain event, the wood moisture content at the surface is above the corrosion threshold; the depth of this high moisture region is dependent on the amount of rainfall and duration of the rain event. At depths far below the surface, the moisture content is not affected by the rain and remains below the corrosion threshold. In between these two locations, moisture is transported into the wood by diffusion and a gradient of moisture content is expected. Also, following a rain event, the wood begins to dry out from the surface, and surface drops quite quickly below the corrosion threshold. After the rainfall stops, the first few mm of the wood are at the capillary saturation threshold moisture content, which is why the maximum is not at the surface that gets wet by rain, but a short distance below it.

An example of the relationship between moisture content and rain events is given in Fig. 5, which plots the hourly precipitation and moisture content for one month (April) using the Baltimore climate data. The data are taken at 1.8 mm below the fastener surface, where the maximum yearly average moisture content occurred for this city. At this depth, the moisture content reaches a maximum quickly after a rain event (in a few hours), and then dries out over tens of hours. Another illustration of the effect of precipitation on the moisture content, and therefore corrosion, is

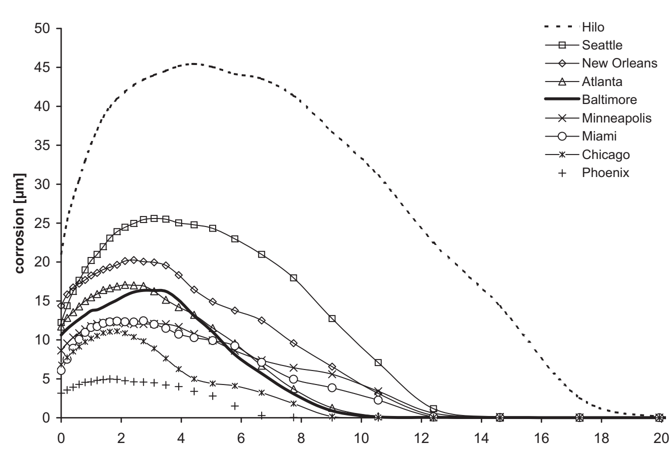

Fig. 4. Amount of corrosion after one year as a function of depth below the wood surface for each of the climates simulated.

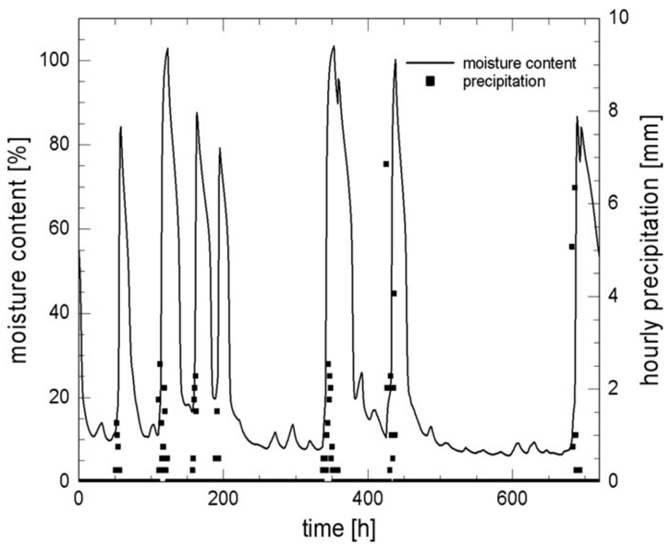

Fig. 5. Hourly calculated moisture contents 1.8 mm below the fastener surface as a function of time for the month of April using the Baltimore climatic data. Precipitation is included on the second axis.

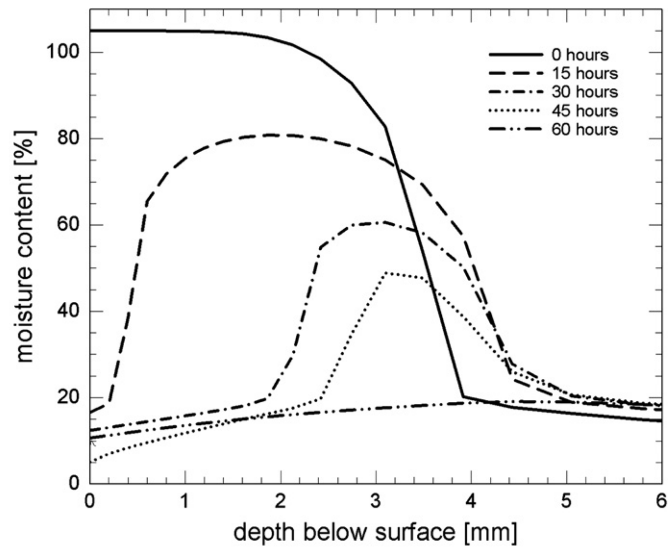

Fig. 6. Moisture content profile as a function of time after a rain event (corresponding to ∼350 h in Fig. 5).

given in Fig. 6, which plots the entire moisture profile after the rain event corresponding to approximately 350 h in Fig. 5 (time = 0 in Fig. 6 corresponds to time = 353 in Fig. 5). After 60 h, the peak in the moisture content graph has disappeared.

To make comparisons between the cities easier, the maxima of the curves in Fig. 4 have been tabulated in Table 1. As expected, Hilo, with over 5 m of rainfall, has the most corrosion and Phoenix, with less than 0.4 m, is the environment leading to the least corrosion. After Hilo, Seattle has the next highest corrosion rate. This city, while relatively low in annual rainfall, has 50% more hours with a rain event than the next highest city (Baltimore).

Surprisingly, Miami and New Orleans, which have the same total rainfall (2.12 m) and nearly the same number of hours (588 vs 593 h) of precipitation, have very different amounts of corrosion (67% difference). Since this behavior cannot be explained in terms of the annual totals in Table 1, the rain events are plotted as a time series in Fig. 7. From this figure, it qualitatively appears that the rain events in New Orleans are spread more evenly throughout the year whereas the Miami rain events appear more concentrated between hours 3000 and 8000. This difference in distribution of rain throughout the year could explain the differences in corrosion between these two cities. Likewise, Chicago and Minneapolis have a similar number of hours of rain, but Chicago has more rain (1.25 m as opposed to 0.99 m) and more hours with the air temperature above freezing, yet the simulation results indicate slightly less corrosion for Chicago than for Minneapolis.

The corrosion profiles had a similar shape in all climates with a maximum 2–5 mm below the wood surface. The fact that no corrosion is observed at 10–20 mm below the surface is a result of the relatively low starting moisture content. After the lumber is preservative treated, it is completely saturated with water and preservative chemicals. Although best construction practices suggest that the wood should be kiln dried after treatment and before construction, in reality, decks are frequently built from lumber that is still wet from treating. To simulate the effect of a "built-wet" construction, a simulation was run for Baltimore with the wood starting in a capillary saturated state. This analysis assumes that the freshly treated lumber is chemically the same as dried and rewetted lumber. The corrosion profile is shown as a function of time in Fig. 8, along with the 1 year data with a 13% starting moisture content shown as a baseline. The corrosion profile after 3 months is nearly uniform at ∼3 μm and represents the corrosion that occurred from the initially high moisture content. After the first three months, the amount of corrosion remains at 3 μm, as the wood has dried to below the corrosion threshold corrosion is dominated by precipitation. This analysis suggests that while building with freshly treated lumber increases corrosion, it only affects the first few months after construction and should have a small effect compared to atmospherically induced corrosion.

4. Discussion

The combined model was used to determine the corrosion profile of metal fasteners embedded in wood for several different climates. Here, we discuss issues relating to the selection of

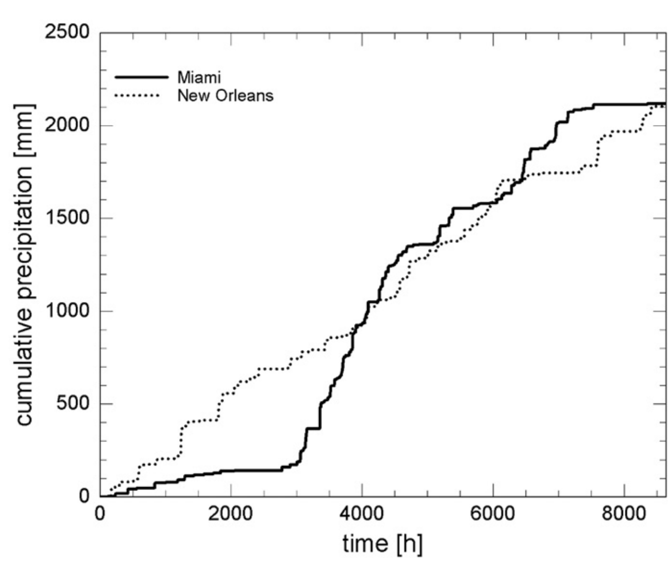

Fig. 7. Cumulative precipitation as a function of time of the year for Miami and New Orleans.

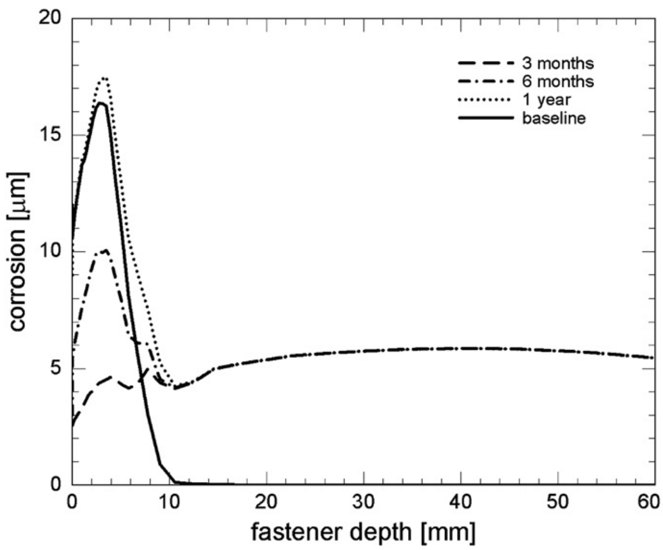

Fig. 8. Corrosion profile for Baltimore where the initial moisture content was set at saturation after 3, 6 and 12 months compared with the baseline simulation with an initial moisture content of 13%.

a reference year for corrosion and the sensitivity of the corrosion model parameters.

4.1. Selection of the reference year

The results show that the corrosion of fasteners depends on the environmental loading. Although only the amount and number of hours of rain are examined in selecting the reference years, there is not a strict correlation between either of these variables and the simulated corrosion. This suggests that other climatic variables are also affecting the corrosion of metals in wood in outdoor exposure. While there has been much work on selecting reference years for analysis of building envelope assemblies [29–36], and using climate year data to assess rain loads [36–38], the moisture loads on exterior structures have not been assessed so systematically. Structures such as decks are clearly different from walls as they receive the entire amount of horizontal rainfall, and do not have interior/exterior temperature and moisture gradients.

The method for selecting the years is based on the results of a few preliminary simulations, which are used to select the important climatic variables, and then deduce what parameters should be used to select the climate years. However, the results of simulations in different climates with nearly the same controlled climate parameters produce different corrosion rates, which suggests that not all of the physics is captured in the original parameters used to select reference years. A more systematic approach seems warranted for the selection of reference years for outdoor structures.

4.2. Examination of the sensitivity of the corrosion model

The corrosion profile is the result of two models: a hygrothermal model that determines the wood moisture content and temperature distribution over the calculation domain, and a corrosion model that translates this moisture content into a corrosion rate at the nail surface. While hygrothermal models have been developed and improved for many years, this work presents a first model relating wood moisture content to a corrosion rate. There are only a few examples in the literature where corrosion was examined as a function of moisture content or relative humidity. Because of the limited quality of the data used to construct the corrosion model, the sensitivity of the corrosion profile to the corrosion model parameters is here examined.

The sensitivity of the corrosion rate as a function of moisture content is examined by running simulations for Baltimore where only the corrosion function (Eq. (1)) is varied. The parameter A is not studied, as it changes the whole corrosion profile proportionally; that is, if A were doubled, the result would be doubling the entire corrosion profile. The parameter B, physically the width of the distribution, is varied from 0.1 to 2 from an original value of 0.83 (Fig. 9a). The threshold value, represented by C, is varied from 14 to 34 from an original value of 24 (Fig. 10a); results are shown in Figs. 9b and 10b.

Of the two parameters, the corrosion profile is less sensitive to B. Increasing B from 0.83 to 2 results in nearly no change in the profile. Intuitively, this can be expected because B represents the steepness of the transition. Because the original function already had a steep transition, and the function approaches the Heavyside function as B gets arbitrarily large, the corrosion profile is nearly at its limiting case to begin with. Decreasing B causes an increase in the total corrosion and a smoothing of the transition from the corrosion maximum to the lowest amount of corrosion. At the lowest values shown, corrosion occurs along the entire length of the fastener. However, a close examination of Fig. 9a reveals that in these cases, the corrosion rate is non-zero at very low moisture contents, which may be unphysical. For example, Baechler measured no corrosion

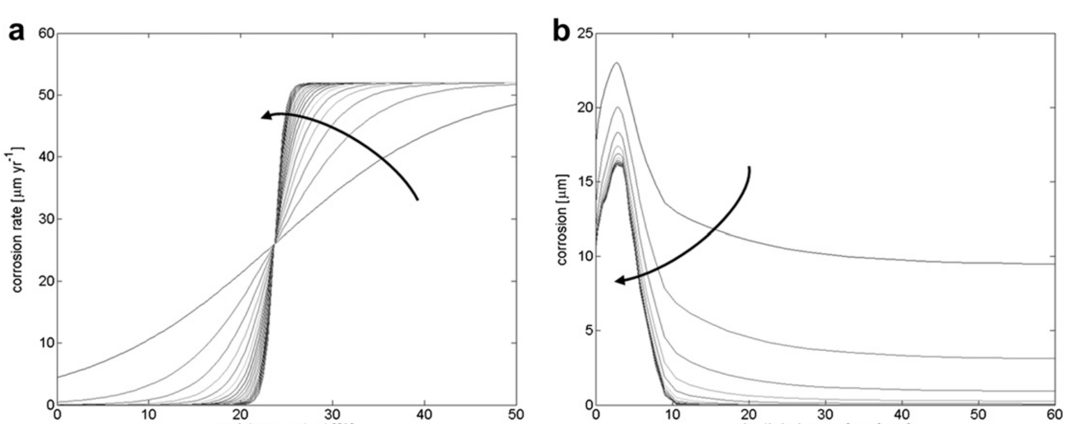

Fig. 9. Effect of changing B on the corrosion rate as a function of moisture content (a) and the resulting corrosion depth profile in a one year simulation for Baltimore (b). B was varied from 0.1 to 2 in increments of 0.1 (compared with the original value of 0.83). The arrows point in the direction of increasing B.

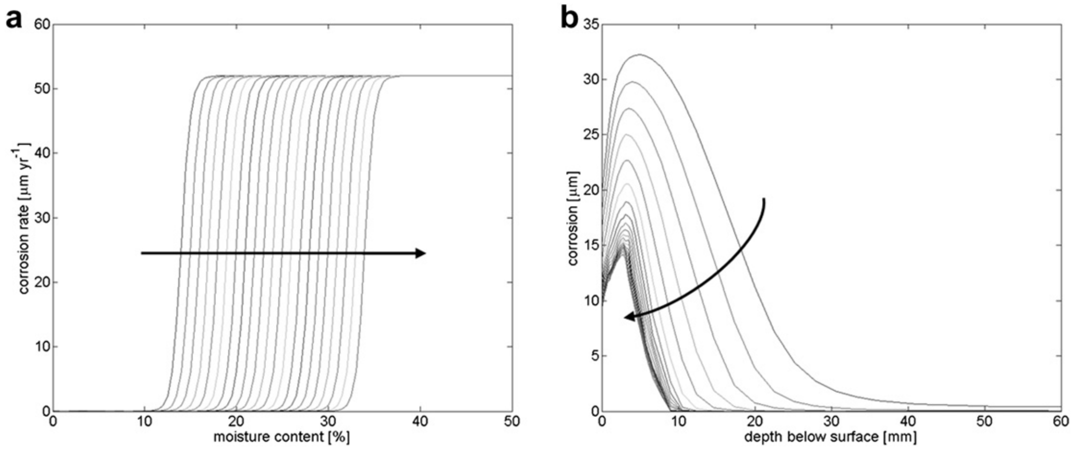

Fig. 10. Effect of changing *C* on the corrosion rate as a function of moisture content (a) and the resulting corrosion depth profile in a one year simulation for Baltimore (b). *C* was varied from 14 to 34 in increments of 1 (compared with the original value of 24). The arrows point in the direction of increasing *C*.

for metals embedded in wood at 27 °C and 65%RH (∼12%MC) for 20 years [39]. In short, it appears that within physical limits, the corrosion profile is not highly sensitive to *B*.

The parameter *C*, a measure of the transition moisture content, affects both the shape and magnitude of the corrosion profile. As *C* is increased to higher moisture contents, the curve retains it shape; however, the corrosion maximum is decreased and the depth at which there is no corrosion moves toward smaller values. Even with a threshold value of 34% MC, which is greater than the fiber saturation point of southern pines where free water exists in the lumina [40], the corrosion profile retains it shape. As *C* is decreased to lower moisture contents, the profile increases in magnitude and begins to broaden. The maximum in the corrosion profile increases rapidly as the threshold decreases, nearly doubling as the threshold is lowered from 24 to 14.

In summary, the corrosion profile is much more sensitive to the moisture content threshold of corrosion, i.e. parameter *C*, than to the steepness of the corrosion model, parameter *B*. As *B* increases, the corrosion rate as a function of moisture content approaches a Heavyside function, which would only require two parameters. The goal of this sensitivity analysis was to aid future experiments determining the corrosion rate function. From this analysis, it appears that most of the work should involve carefully determining the corrosion threshold by focusing the measurements around this value rather than taking measurements over a broad range of moisture contents to precisely observe the distribution.

5. Conclusions

This paper presents a combined hygrothermal/corrosion model for simulating the corrosion of metals embedded in wood. The model is developed to aid in the design of wood/metal assemblies used in exterior construction. Several US cities are examined with the model using reference years based upon precipitation. Although in general cities with a high annual rainfall or number of hours of rain exhibit high corrosion, there are several exceptions.

The simulations show that in most cases, corrosion is confined to the first 10 mm below the wood surface. The highest corrosion occurs 1–5 mm below the surface of the wood. For built-wet construction, the simulated wood joist dries to below the corrosion threshold within the first 3 months. The sensitivity of the function that relates moisture content to corrosion is examined. It is found that the corrosion profile is more sensitive to the corrosion threshold than the width of the transition from no corrosion to the maximum corrosion rate.

There are several logical extensions to the currently presented work. First, the combined model could be compared with a field corrosion test that includes monitoring of environmental conditions and wood moisture content. Second, the hygrothermal properties of ACQ-treated southern pine could be better characterized, including temperature dependencies. Third, the corrosion model could be improved with further experiments to locate the corrosion threshold. Finally, it may be worthwhile to develop a more systematic method for selecting reference years for exterior structures.

Acknowledgments

The authors acknowledge funding from the US. Federal Highway Administration under the Cooperative Research Program for Covered Bridges. The authors are grateful for the contributions and support of Jan Carmeliet and Hannelore Derluyn (Chair of Building Physics, ETH Zürich, Switzerland), Peter Moonen (Empa, Dübendorf, Switzerland), and C.R. Boardman (US Forest Products Laboratory, Madison, WI, USA).

References

[1] Lebow S. Alternatives to chromated copper arsenate for residential construction. Res. Pap. FPL-RP-618. Madison, WI: U.S.D.A. Forest Service, Forest Products Laboratory; 2004.
[2] Burkholder M. CCA, NFBA, and the post-frame building industry. Frame Building News 2004;16:6–12.
[3] Anon. Preservative treated wood. Simpson Strong-Tie Technical Bulletin; 2008.
[4] Freeman MA, McIntyre CR. A comprehensive review of copper-based wood preservatives with a focus on new micronized or dispersed copper systems. Forest Products Journal 2008;58:6–27.
[5] Kear G, Wu H-Z, Jones MS. Weight loss studies of fastener materials corrosion in contact with timbers treated with copper azole and alkaline copper quaternary compounds. Corrosion Science 2009;51:252–62.
[6] Zelinka SL, Rammer DR. Corrosion rates of fasteners in treated wood exposed to 100% relative humidity. ASCE Journal of Materials in Civil Engineering 2009; 21:758–63.
[7] Zelinka SL, Rammer DR, Stone DS. Electrochemical corrosion testing of fasteners in wood extract. Corrosion Science 2008;50:1251–7.
[8] Lebow S, Lebow P. The role of moisture in above-ground leaching. Jackson Hole, Wyoming, USA: IRG Secretariat; 2007.
[9] Glass SV, TenWolde A. Review of in-service moisture and temperature conditions in wood-frame buildings. Gen. Tech. Rp. FPL-GTR-174. U.S. Department of Agriculture, Forest Service, Forest Products Laboratory; 2007.

[10] Janssen H, Blocken B, Carmeliet J. Conservative modelling of the moisture and heat transfer in building components under atmospheric excitation. International Journal of Heat and Mass Transfer 2007;50:1128–40.
[11] Baker AJ. In: Hamel M, editor. Corrosion of metals in preservative-treated wood. Memphis, TN: Forest Products Research Society; 1987. p. 99–101.
[12] Short NR, Dennis JK. Corrosion resistance of zinc-alloy coated steel in construction industry environments. Transactions of the Institute of Metal Finishing 1997;75:47–52.
[13] Dennis JK, Zou C, Short NR. Corrosion behaviour of zinc and zinc alloy coated steel in preservative treated timber. Transactions of the Institute of Metal Finishing 1995;75:96–101.
[14] Duncan JR. Corrosion of metal fasteners in timber. Construction Building Materials 1988;2:194–200.
[15] Anon. ISO 9223 corrosion of metals and alloys- corrosivity of atmospheres-classification. Geneva, Switzerland: International Organization for Standardization; 1992.
[16] Mansfeld F. Tafel slopes and corrosion rates from polarization resistance measurements. Corrosion 1973;29:397–402.
[17] Poupard O, Aït-Mokhtar A, Dumargue P. Impedance spectroscopy in reinforced concrete: procedure for monitoring steel corrosion part I: development of the experimental device. Journal of Materials Science 2003;38: 2845–50.
[18] Poupard O, Aït-Mokhtar A, Dumargue P. Impedance spectroscopy in reinforced concrete: experimental procedure for monitoring steel corrosion part II: polarization effect. Journal of Materials Science 2003;38:3521–6.
[19] Aït-Mokhtar A, Poupard O, Dumargue P. Relationship between the transfer properties of the coating and impedance spectroscopy in reinforced cement-based materials. Journal of Materials Science 2006;41:6006–14.
[20] Janssen H, Carmeliet J, Hens H. The influence of soil moisture transfer on building heat loss via the ground. Building and Environment 2004;39: 825–36.
[21] Janssen H, Blocken B, Roels S, Carmeliet J. Wind-driven rain as a boundary condition for HAM simulations: analysis of simplified modelling approaches. Building and Environment 2007;42:1555–67.
[22] Zelinka SL, Glass SV. Water vapor sorption isotherms for southern pine treated with several waterborne preservatives. ASTM Journal of Testing and Evaluation 2010;38:80–8.
[23] Zillig W, Janssen H, Carmeliet J, Derome D. Liquid water transport in wood: towards a mesoscopic approach. In: Fazio P, Ge H, Rao J, Desmarais G, editors. Research in Building Physics and Building Engineering. London: Taylor and Francis Group; 2006.
[24] Carmeliet J, Janssen H, Derluyn H. An improved moisture diffusivity model for porous building materials; 2007. Desden, Germany.
[25] Glass SV, Zelinka SL. In: Ross RJ, editor. Wood handbook, wood as an engineering material. Moisture relations and physical properties of wood. U.S. Department of Agriculture, Forest Service, Forest Products Laboratory; 2010.
[26] Zelinka SL, Derome D, Glass SV. From laboratory corrosion tests to a corrosion lifetime for wood fasteners: progress and challenges. In: Proceedings of the International Convention of Society of Wood Science and Technology and United Nations Economic Commission for Europe- Timber Committee. Geneva, Switzerland: SWST; 2010. p. WS-96.
[27] Briggs RS, Lucas RG, Taylor ZT. Climate classification for building energy codes and standards. Chicago, IL: American Society of Heating, Refrigerating and Air-Conditioning Engineers (ASHRAE); 2003.
[28] Anon. Solar and meteorological surface observational network (SAMSON), 1961-1990. Asheville, North Carolina: National Climatic Data Center (NCDC); 1993. 3 Volume CD-ROM set.
[29] ASHRAE. ANSI/ASHRAE Standard 160-2009. Criteria for moisture-control design analysis in buildings. Atlanta: American Society of Heating, Refrigerating and Air-Conditioning Engineers, Inc.; 2009.
[30] Salonvaara M, Sedlebauer K, Holm A, Pazera M. Effect of selected weather year for hygrothermal analyses. In: Proceedings of thermal performance of the exterior envelopes of whole buildings XI. Atlanta: American Society of Heating, Refrigerating and Air-Conditioning Engineers, Inc.; 2010.
[31] Cornick S, Djebbar R, Dalgliesh WA. Selecting moisture reference years using a moisture index approach. Building and Environment 2003;38:1367–79.
[32] Sanders C. Environmental conditions, final report: task 2. Energy conservation in buildings and community systems, Annex 24 heat-air and moisture transfer in Insulated envelope Parts (HAMTIE). Laboratorium Bouwfysica, K.U.-Leuven, Belgium: International Energy Agency; 1996.
[33] David M, Adelard L, Lauret P, Garde F. A method to generate typical meteorological years from raw hourly climatic databases. Building and Environment 2010;45:1722–32.
[34] Kershaw T, Eames M, Coley D. Assessing the risk of climate change for buildings: a comparison between multi-year and probabilistic reference year simulations. Building and Environment 2011;46:1303–8.
[35] Zhu D, Reddy Mallidi S, Fazio P. Approach for urban driving rain index by using climatological data recorded at suburban meteorological station. Building and Environment 1995;30:229–36.
[36] Blocken B, Carmeliet J. Overview of three state-of-the-art wind-driven rain assessment models and comparison based on model theory. Building and Environment 2010;45:691–703.
[37] Blocken B, Carmeliet J. Validation of CFD simulations of wind-driven rain on a low-rise building facade. Building and Environment 2007;42:2530–48.
[38] Abuku M, Blocken B, Nore K, Thue JV, Carmeliet J, Roels S. On the validity of numerical wind-driven rain simulation on a rectangular low-rise building under various oblique winds. Building and Environment 2009;44:621–32.
[39] Baechler RH. Corrosion of metal fastenings in zinc-chloride treated wood after 20 years. St. Louis, MO: American Wood Preservers' Association; 1949. pp. 381–97.
[40] Stamm AJ. The fiber-saturation point of wood as obtained from electrical conductivity measurements. Industrial and Engineering Chemistry, Analytical Edition 1929;1:94–7.